

Nonequilibrium phononic first-order phase transition in a driven fermion chain

Mohsen Yarmohammadi,^{1,*} Marin Bukov,^{2,†} and Michael H. Kolodrubetz^{1,‡}

¹*Department of Physics, The University of Texas at Dallas, Richardson, Texas 75080, USA*

²*Max Planck Institute for the Physics of Complex Systems, Nöthnitzer Str. 38, 01187 Dresden, Germany*

(Dated: April 26, 2023)

We study the direct laser drive of infrared-active phonons that are quadratically coupled to a spinless fermion chain. Feedback is incorporated by phonon dressing of the electronic dispersion, which enables effective non-linearities in the phonon dynamics. We uncover a first-order phase transition in the phononic steady state in which hysteretic effects allow either large or small phonon occupation depending on the drive protocol. We discuss the implications of these findings for probing phase transitions in real driven materials.

Introduction.—Despite a considerable ongoing effort to understand quantum systems, uncovering nonequilibrium phenomena without an apparent equilibrium analogue is one of the outstanding scientific challenges in modern condensed matter physics. Recent developments in the ultrafast dynamics of quantum materials have attracted interest in exploring novel nonequilibrium many-body phenomena [1–7]. Interacting light-matter systems with competing interactions emerged as a useful experimental platform since they allow to study the interplay between coupling to an environment and external drives [8–10]. Moreover, they play a central role in the study of photovoltaics [11, 12], light-induced phase transitions [13, 14], and laser processing [15].

Direct laser driving of an infrared (IR)-active phonon is the main light-matter interaction channel; it couples to the electron degree of freedom by modifying its environment. In a typical setup, phonons couple to the electron number operator in a nonlinear manner [16]. Over the last decade, a considerable effort has been devoted to studying the role of electron-phonon coupling on the dynamical properties of high-temperature cuprate superconductors [17, 18] and Mott or charge-density-wave insulators [19–22]. For a driven electron-phonon system to avoid heating (e.g., with the goal to store and transmit information), the latter needs to be counterbalanced by dissipation from undriven phonon modes. This has been studied in spin lattices [23–25], coupled quantum-electrodynamics cavities and circuits [26–28], lattice Rydberg atoms [29–31], driven-dissipative superfluids [32], nonlinear photonic modes [33, 34], etc. Although dissipation is widely captured in the dynamics of local observables, a detailed understanding of the process is still an outstanding challenge.

Studies of interacting systems, exposed to an external laser field and coupled to a thermal bath, have until recently mostly focused on the “bare” dispersion of degrees of freedom in dissipation processes. However, it remains to be understood how the backaction of transient excitations can be incorporated into the dissipation process. To the best of our knowledge, this has not been addressed so far in phononically driven materials. This mainly requires a deep scan of the “dressed” electronic dispersion

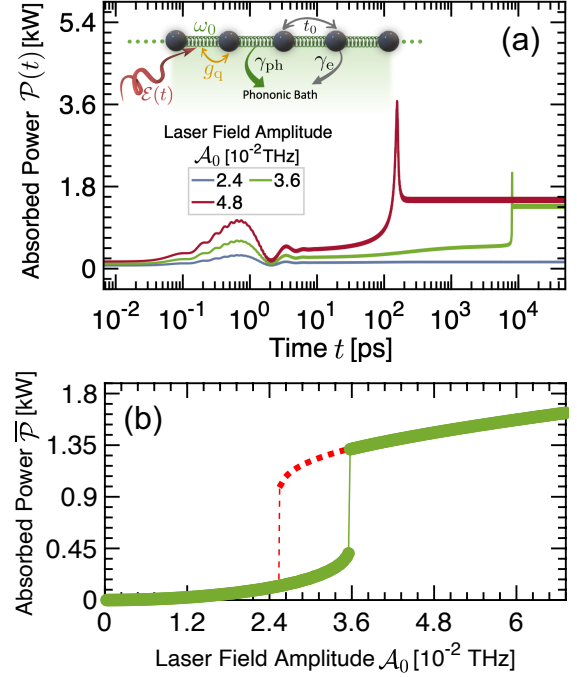


FIG. 1. Nonequilibrium first-order phase transition in a phononically driven fermion chain. (a) Drive-period-averaged time evolution of absorbed power for a driven-dissipative chain of spinless fermions, sketched in the inset, starting from the ground state at half filling. The system reaches a nonequilibrium steady state (NESS) which undergoes a first-order phase transition at laser amplitude $\mathcal{A}_0 \approx 3.6 \times 10^{-2}$ THz [solid line in (b)] due to phononic modification of the electronic dispersion. The dashed line in (b) shows a second stable NESS which can be created by modifying either the initial state or drive protocol. The parameters are chosen to be $\omega = 4.44$ THz, $\omega_0 = 4.8$ THz, $g_q = 9.6$ THz, $\gamma_{ph} = 0.24$ THz, and $\gamma_e = 0.0024$ THz; see text for details.

through a time-dependent damping rate, which results in a novel physical insight.

In this Letter, we show that a driven-dissipative fermion chain with a dressed dispersion, exhibits a *dynamical first-order phase transition* due to local depopulation of the electrons in the spirit of quadratic electron-phonon coupling (QEPC). One experimental signature of

the transition is a sharp spike in the long time-evolution of the absorbed power, accompanied by a discontinuity in its value in the long-time nonequilibrium steady state (NESS), as shown in Fig. 1. We analyze and identify accessible parameter regimes to provide a clear path for experimental verification.

Model.—Consider an infinite half-filled chain of spinless fermions with periodic boundary conditions, as illustrated in Fig. 1(a), inset. We drive the chain by a continuous field coupled to the IR-active optical phonons, which illuminates the entire system until it reaches a NESS. The model Hamiltonian reads [35–37]

$$\mathcal{H}(t) = -t_0 \sum_{\ell} (c_{\ell}^{\dagger} c_{\ell+1} + \text{H.c.}) + \omega_0 \sum_{\ell} a_{\ell}^{\dagger} a_{\ell} + g_q \sum_{\ell} (a_{\ell}^{\dagger} + a_{\ell})^2 (c_{\ell}^{\dagger} c_{\ell} - 1/2) + \mathcal{E}(t) \sum_{\ell} (a_{\ell}^{\dagger} + a_{\ell}), \quad (1)$$

where c_{ℓ}^{\dagger} (c_{ℓ}) and a_{ℓ}^{\dagger} (a_{ℓ}) are respectively the electron and phonon creation (annihilation) operators at lattice site ℓ ; t_0 is a constant hopping amplitude setting the energy scale of our model, ω_0 is the optical phonon frequency, $c_{\ell}^{\dagger} c_{\ell} - 1/2$ is the electron number operator relative to half filling, and g_q is the QEPC strength. In the laser-phonon coupling, the laser field is described by $\mathcal{E}(t) = \mathcal{A}_0 \cos(\omega t)$ with frequency ω and amplitude \mathcal{A}_0 . In momentum space, we have the bare electronic dispersion $\omega_k = -2t_0 \cos k$ and a k -independent phonon frequency; the full k -space Hamiltonian is provided in Sec. S1 of the Supplemental Material (SM) [38].

We focus our simulations on the dynamics of the approximate dispersionless phonon (assuming a flat band for Einstein phonons), since in most materials the average ω_0 is much larger than the phonon bandwidth. Due to the relatively long wavelength of the drive phonons compared to the lattice spacing, the phonon response is dominated by the zero momentum mode a_0 . We also neglect linear and higher electron-phonon coupling effects, since in target centrosymmetric structures [36, 37] the dominant coupling is quadratic. For comparison to experiments on materials with nonlinear electron-phonon coupling, we choose to consider a representative hopping energy $t_0 = 10 \text{ meV} \approx 2.4 \text{ THz}$, which can also be chosen to be similar to $(\text{Pb,Bi})_2\text{Sr}_2\text{CaCu}_2\text{O}_8$, $\text{YBa}_2\text{Cu}_3\text{O}_{6+x}$, and K_3C_{60} [36, 39–41] without qualitatively modifying the results.

The system is coupled to a phononic bath (given by independent phonon modes not subject to the drive) which allows the formation of a NESS. To model the dynamics of the dissipation process, we use the Lindblad master equation with conventional local jump operators, (a_0^{\dagger}, a_0) and (c_k^{\dagger}, c_k) , and decoherence rates, γ_{ph} and γ_e , which relax the phonons and electrons, respectively, to thermal equilibrium [25, 42–44]. We consider relaxation toward zero temperature which, crucially, depends on the state of the phonons and electrons via the QEPC. Therefore, as the phonon fluctuations $(a_0^{\dagger} + a_0)^2$ become large, they

shift the chemical potential of the electrons downward, modifying the NESS electron density in the region where the laser drive couples. Moreover, we assume that the chain is in touch with a cooling apparatus [25] to remediate the heating created by the continuous drive. Although our results are robust to the parameters chosen, we consider the experimentally relevant $\omega_0 = 4.8 \text{ THz}$, $\gamma_{\text{ph}} = 0.24 \text{ THz}$, and $\gamma_e = 0.0024 \text{ THz}$ throughout the text, unless otherwise specified.

We initialize the system in its ground state (electrons at half filling, phonons in the vacuum state), and let it evolve in time following the Lindblad formalism [42, 43]. We perform numerical simulations for chain lengths up to $L = 1001$ sites. A complete derivation of the equations of motion governing the time evolution of the system’s observables can be found in Sec. S2 of the SM.

As the QEPC g_q plays an essential role in determining the dynamics of the model, it is worth noting that the renormalization of the phonon frequency in our model, i.e., $\tilde{\omega}_0 = \omega_0 \sqrt{1 + 4g_q[\langle n_{e,\ell} \rangle - 1/2]}/\omega_0$ does not lead to instabilities in the simulation, in contrast to other works [36, 37] where the system is unstable for $|g_q| > \omega_0/2$. The reason for this is our mean-field-type approximation, which replaces the quantized on-site electron occupation by an average value that only weakly deviates from $1/2$. Crucially, this lack of instability is also physical, suggesting that our results will survive fluctuations. This is because the constraint $|g_q| > \omega_0/2$ comes from the assumption of dispersionless Einstein phonons; in reality, there will always be some finite dispersion, causing excitations of the phonons to be spread over at least a few sites. If the minimal spatial dispersion is ℓ sites, the instability threshold should be roughly increased by a factor of ℓ , which brings it well above the value for g_q in real materials. Hence, our approximation allows us to simulate the model for arbitrary QEPC strength.

Results.—Upon quenching on the drive and solving the dynamics, the system evolves into a NESS as seen in Fig. 1(a) and Sec. S3 of the SM. For the majority of parameters, it takes around 600 ps to reach the NESS, which is within the current technological capabilities of laser sources in ultrafast experiments. To remove fast oscillations, we often average an observable $O(t)$ over one drive period, denoted by \bar{O} . In addition to microscopic parameters such as electron and phonon occupation, we consider the NESS energy flow from the drive into the final stage of dissipation for various degrees of freedom (see Sec. S4 of the SM). Of particular importance is the absorbed power

$$\mathcal{P}(t) = -w a \rho \omega_0 \mathcal{E}(t) p_{\text{ph}}(t), \quad (2)$$

where $p_{\text{ph}}(t) = L^{-1/2} \langle i(a_0^{\dagger} - a_0) \rangle(t)$ denotes the phonon momentum. We use parameters from the YBCO sample [45], namely thickness $w = 10 \text{ nm}$, area $a = 1 \text{ mm}^2$, and molar density $\rho \approx 0.007 \text{ mol.cm}^{-3}$. This power is

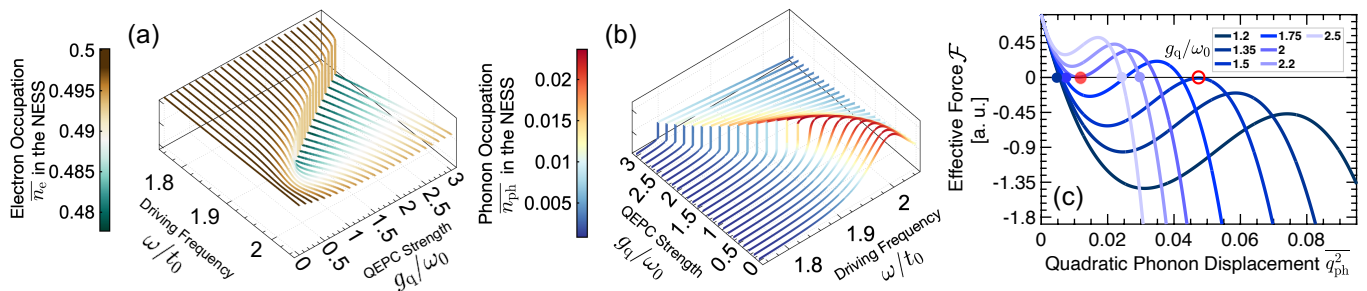


FIG. 2. **Origin of nonequilibrium first-order phase transition.** Dynamical response of dressed (a) electron and (b) phonon occupations in the nonequilibrium steady state for various quadratic electron-phonon couplings and driving frequencies (axes are swapped in (b) to improve visibility of jumps at the phase transition). Depopulation of the electrons leads to shifting of the phonon resonance, a nonlinearity which enables a first-order phase transition in the NESS at strong g_q . (c) Nonequilibrium effective force (see text) for various g_q at driving frequency $\omega = 4.44$ THz, which is below the bare phonon frequency. Shaded blue dots indicate the numerical steady state. Red dots indicate the two predicted phase transitions (see text), with bistability for $3/2 < g_q/\omega_0 < 2$. Parameters are $\omega_0 = 4.8$ THz, $\mathcal{A}_0 = 0.036$ THz, $\gamma_{\text{ph}} = 0.24$ THz, and $\gamma_e = 0.0024$ THz.

related to experimentally measurable quantities such as reflectance [46–53].

We begin by discussing the response of the electrons and phonons to changing drive frequency ω and QEPC g_q [Figs. 2(a) and 2(b)]. In the absence of QEPC, there is a resonant peak at $\omega = \omega_0$, more clearly visible in the phonon occupation. As g_q is increased, the peak shifts to the lower frequency, which comes from the depopulation of the electronic modes via feedback from the phonons. Surprisingly, above a critical value of g_q , the smooth peak suddenly becomes a sharp jump, suggestive of a first-order phase transition. At this transition point, the time-evolved observables undergo a non-analytic change, exhibiting a sharp peak at long times as seen in Fig. 1(a).

As we show later, modifying either the initial state or the drive protocol leads to a different NESS, as shown by the dashed red line in Fig. 1(b) and supported by the data in Fig. 4.

The main origin of the phase transition is dissipation-induced nonlinearity. The dressed electron dispersion $\tilde{\omega}_k(t) = \omega_k + g_q q_{\text{ph}}^2(t)$ will yield an average shift of the electron chemical potential given by $g_q \overline{q_{\text{ph}}^2}$, where $q_{\text{ph}}(t) = L^{-1/2} \langle a_0^\dagger + a_0 \rangle(t)$ is the phonon displacement. Defining the electron density $n_e(t) = L^{-1} \sum_k \langle c_k^\dagger c_k \rangle(t)$ and linearizing around the Fermi surface, we predict a steady state electron density of

$$\bar{n}_e = \frac{1}{2} - \frac{g_q \overline{q_{\text{ph}}^2}}{2\pi t_0}. \quad (3)$$

Similarly, the electron occupation shifts the effective phonon frequency to $\tilde{\omega}_0(t) = \omega_0 \sqrt{1 + 4g_q [n_{e,k}(t) - 1/2] / \omega_0}$ [54]. Since the steady state to which the electrons attempt to relax to depends on the phonon state, whose dynamics, in turn, depend on the electron density, this results in effective nonlinearities in the dynamics. This backaction was not considered in previous works [36, 37] because the electron was assumed to relax to its undriven ground state.

While reasonable for linear electron-phonon coupling, the presence of a finite q_{ph}^2 makes this backaction crucial for QEPC through the Fermi-Dirac mean number [55]. Correctly accounting for this backaction is our major contribution to the model which, as we have seen, produces significant effects on the dynamics. It is also important to note that $q_{\text{ph}}^2(t)$ can be experimentally measured through the intensity of a diffraction peak in femtosecond time-resolved X-rays [56], enabling another path to measure the effects of this backaction.

To microscopically interpret the observed phase transition, we consider the system near its steady state; we assume that the phonons synchronize with the drive, with complex Fourier component of displacement $q_1 e^{i\omega t}$, where $q_{\text{ph}}^2 = |q_1|^2/2$. Away from the NESS, q_1 slowly evolves towards a stationary point, which can be obtained by setting $\dot{q}_{\text{ph}} = 0$. As shown in Sec. S5 of the SM, this gives a cubic equation that may be thought of as an effective force acting on the phonon near the NESS:

$$\mathcal{F}(\mathcal{X}) = -\frac{4g_q^4 \omega_0^2}{\pi^2 t_0^2} \mathcal{X}^3 - \frac{4g_q^2 \omega_0}{\pi t_0} \left(\omega^2 - \omega_0^2 + \frac{\gamma_{\text{ph}}^2}{4} \right) \mathcal{X}^2 - \left(\gamma_{\text{ph}}^2 \omega^2 + (\omega^2 - \omega_0^2)^2 \right) \mathcal{X} + 2\mathcal{A}_0^2 \omega_0^2, \quad (4)$$

where $\mathcal{X} = \overline{q_{\text{ph}}^2}$. Steady states out of equilibrium correspond to solutions of $\mathcal{F}(\mathcal{X}) = 0$; stable attractors have $d\mathcal{F}/d\mathcal{X} < 0$. As seen in Fig. 2(c), the force curve shifts depending on various parameters and can be tuned from having a unique NESS to a regime with two distinct stable NESSs. As seen in Fig. 2(c), the force curve shifts depending on various parameters and appears to have two separate phase transitions (marked by red circles) from having a unique NESS to a regime with two distinct stable NESSs. The first phase transition (transparent circle) is visible in our numerical data since, starting from a vacuum state, a jump from small to large q_{ph}^2 matches our expectations. The second phase transition (open circle) is not seen in the data, but could be realized via protocols similar to those in Fig. 4. This bifurcation transition

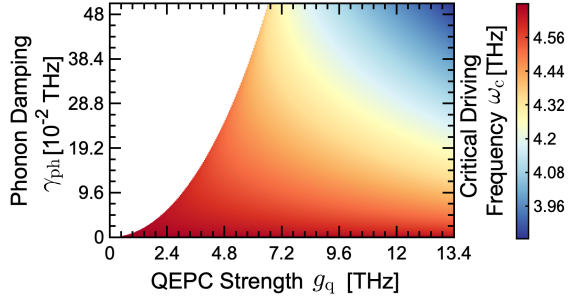


FIG. 3. **Dynamical damping-coupling constraint for the phase transition.** Critical driving frequency as a function of phonon damping rate and strength of quadratic electron-phonon coupling at $\omega_0 = 4.8$ THz, $\mathcal{A}_0 = 0.036$ THz, and $\gamma_e = 0.0024$ THz. The transition occurs down to arbitrarily small values of g_q and γ_{ph} . The separatrix, below which dynamical first-order phase transitions occur, is parabolic in the $\gamma_{\text{ph}} - g_q$ plane.

with a cubic equation for the effective force is reminiscent of the magnetization in a first-order Ising phase transition. However, we emphasize that our phase transition occurs not in equilibrium, but rather out of equilibrium in the driven NESS.

One may naively conclude from Fig. 2 that the phase transition requires extremely large QEPCs, which can be challenging to find experimentally. However, by solving the cubic equation, we find the following analytical expression for the critical driving frequency:

$$\omega_c = \sqrt{\omega_0^2 - \frac{2\sqrt{3}}{3} \gamma_{\text{ph}} \omega_0 + \frac{1}{2} \sqrt{\gamma_{\text{ph}}^4 - \frac{\pi t_0 \tilde{b}}{3g_q^4 \omega_0} - 4\gamma_{\text{ph}}^2 \omega_0^2 - \frac{96g_q^4 \omega_0^4 \mathcal{A}_0^2}{\pi^2 t_0^2 \tilde{b}}}}, \quad (5)$$

where $\tilde{b} = g_q^2 \omega_0 \gamma_{\text{ph}} (3\gamma_{\text{ph}} - 4\sqrt{3}\omega_0) / \pi t_0$. Importantly, this shows that a phase transition persists down to arbitrarily small g_q , as seen in the parametric plot of γ_{ph} vs. g_q in Fig. 3. Intriguingly, even with 1% damping of phonon energy ($\gamma_{\text{ph}} \approx 0.048$ THz) to the phononic bath, governed by the Lindemann criterion [57], the system still features the phase transition for moderate QEPC $g_q = \omega_0/2 = t_0$. The region in which the transition can be observed increases with the phonon frequency.

The generalized force in Fig. 2(c) suggests that two stable equilibria exist at large g_q or small ω , yet only one NESS is seen in our simulation for each value of the parameters. This is the attractor of the equations of motion starting from our initial ground state. To realize the other NESS, a different initial state must be prepared. Taking the cue from hysteresis near equilibrium first-order phase transitions, we suggest that this may be done via slowly ramping one of the parameters, such as the frequency (a “chirp” protocol). We consider a linearly chirped electric field $\mathcal{E}(t) = \mathcal{A}_0 \cos(\omega(t)t)$ with $\omega(t) = \omega_1 + (\omega_2 - \omega_1)(t - \tau_1) / (\tau_2 - \tau_1)$, as shown in Fig. 4(a), inset. Such frequency ramps are important throughout ultrafast spectroscopy [58, 59], and can thus be imple-

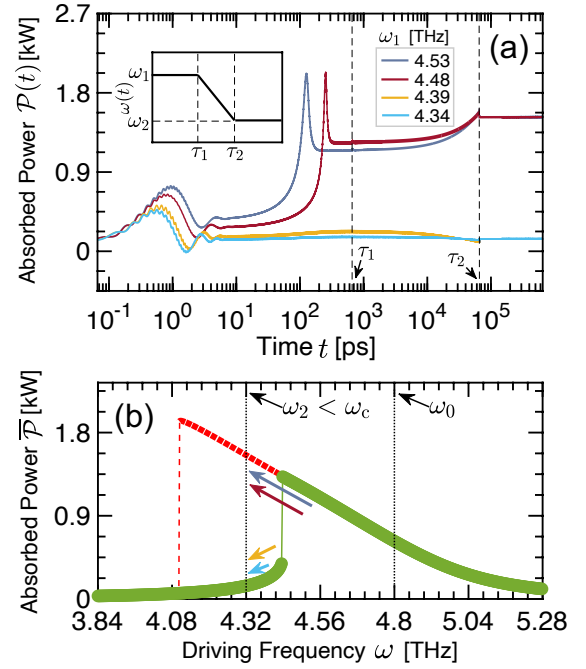


FIG. 4. **Chirp protocol for realizing the alternative steady state.** (a) Absorbed power in presence of a linearly chirped electric field $\mathcal{E}(t) = \mathcal{A}_0 \cos(\omega(t)t)$ with $\omega(t) = \omega_1 + [(\omega_2 - \omega_1)(t - \tau_1) / (\tau_2 - \tau_1)]$ (inset) for fixed $\omega_2 = 4.32$ THz $< \omega_c = 4.44$ THz. (b) Depending on whether ω_1 is less than or greater than ω_c , the system ends up in a different branch of the steady state. Black arrows point to the positions of the frequencies ω_0 and ω_2 (black dotted vertical lines); color-coded arrows indicate the value of ω_1 , cf. legend in (a). Parameters are $\omega_0 = 4.8$ THz, $\mathcal{A}_0 = 0.036$ THz, $\gamma_{\text{ph}} = 0.24$ THz, and $\gamma_e = 0.0024$ THz.

mented experimentally. Starting with frequency ω_1 at time τ_1 sufficiently large to reach the NESS, we slowly ramp to the final value $\omega_2 < \omega_c$ at time τ_2 . If $\omega_1 < \omega_c$ as well, no phase transition is crossed by this ramp and the system simply reaches the original NESS. However, if $\omega_1 > \omega_c$, the system instead stays in the upper NESS with large g_{ph}^2 , as shown in Fig. 4(b). Similar hysteretic preparation of the alternative NESS can be accomplished via slowly ramping other experimental parameters, such as the drive amplitude \mathcal{A}_0 in Fig. 1(b).

Conclusion/Outlook.—We have uncovered a novel nonequilibrium phase transition of a driven-dissipative fermion chain coupled to a phonon mode. By dynamically tuning the dissipation processes through the backaction of phononic excitations on the electronic dispersion, we find a robust phase transition from having a unique nonequilibrium steady state to having two stable steady states. Since the effect is favored by a quasi-equilibrium electron density (less than 2% deviation from a half-filled chain in equilibrium), it should be prevalent in any fermion chain. Our findings motivate future nonequilibrium spectroscopy experiments to seek photo-induced phononic phase transitions in driven quantum materi-

als such as driven superconductors, where the modified phononic steady state may enable a nonequilibrium pathway to controlling superconductivity [60, 61]. This phase transition will likely also be possible in the presence of an electromagnetic cavity, which has been used in recent work to control heating in driven materials [62–64].

Acknowledgments.—This work was performed with support from the National Science Foundation (NSF) through award number DMR-1945529 and the Welch Foundation through award number AT-2036-20200401 (MK and MY). Part of this work was performed at the Aspen Center for Physics, which is supported by NSF grant No. PHY-1607611, and at the Kavli Institute for Theoretical Physics, which is supported by NSF grant No. NSF PHY-1748958. This project was funded by The University of Texas at Dallas Office of Research and Innovation through the SPIRe program. M.B. was supported by Marie Skłodowska Curie Grant No. 890711 (until 01.09.2022).

* mohsen.yarmohammadi@utdallas.edu

† mgbukov@pks.mpg.de

‡ mkolodru@utdallas.edu

- [1] F. Novelli, G. De Filippis, V. Cataudella, M. Esposito, I. Vergara, F. Cilento, E. Sindici, A. Amaricci, C. Giannetti, D. Prabhakaran, S. Wall, A. Perucchi, S. Dal Conte, G. Cerullo, M. Capone, A. Mishchenko, M. Grüninger, N. Nagaosa, F. Parmigiani, and D. Fausti, Witnessing the formation and relaxation of dressed quasiparticles in a strongly correlated electron system, *Nature Communications* **5**, 5112 (2014).
- [2] S. Dal Conte, L. Vidmar, D. Golež, M. Mierzejewski, G. Soavi, S. Peli, F. Banfi, G. Ferrini, R. Comin, B. M. Ludbrook, L. Chauviere, N. D. Zhigadlo, H. Eisaki, M. Greven, S. Lupi, A. Damascelli, D. Brida, M. Capone, J. Bonča, G. Cerullo, and C. Giannetti, Snapshots of the retarded interaction of charge carriers with ultrafast fluctuations in cuprates, *Nature Physics* **11**, 421 (2015).
- [3] C. Giannetti, M. Capone, D. Fausti, M. Fabrizio, F. Parmigiani, and D. Mihailovic, Ultrafast optical spectroscopy of strongly correlated materials and high-temperature superconductors: a non-equilibrium approach, *Advances in Physics* **65**, 58 (2016).
- [4] D. N. Basov, R. D. Averitt, D. van der Marel, M. Dressel, and K. Haule, Electrodynamics of correlated electron materials, *Rev. Mod. Phys.* **83**, 471 (2011).
- [5] J. Orenstein, Ultrafast spectroscopy of quantum materials, *Physics Today* **65**, 44 (2012).
- [6] D. N. Basov, R. D. Averitt, and D. Hsieh, Towards properties on demand in quantum materials, *Nature Materials* **16**, 1077 (2017).
- [7] A. de la Torre, D. M. Kennes, M. Claassen, S. Gerber, J. W. McIver, and M. A. Sentef, Colloquium: Nonthermal pathways to ultrafast control in quantum materials, *Rev. Mod. Phys.* **93**, 041002 (2021).
- [8] I. Carusotto and C. Ciuti, Quantum fluids of light, *Rev. Mod. Phys.* **85**, 299 (2013).
- [9] E. I. R. Chiacchio and A. Nunnenkamp, Emergence of continuous rotational symmetries in ultracold atoms coupled to optical cavities, *Phys. Rev. A* **98**, 023617 (2018).
- [10] N. Lambert, S. Ahmed, M. Cirio, and F. Nori, Modelling the ultra-strongly coupled spin-boson model with unphysical modes, *Nature Communications* **10**, 3721 (2019).
- [11] M. Grätzel, Photoelectrochemical cells, *Nature* **414**, 338 (2001).
- [12] A. D. Wright, C. Verdi, R. L. Milot, G. E. Eperon, M. A. Pérez-Osorio, H. J. Snaith, F. Giustino, M. B. Johnston, and L. M. Herz, Electron-phonon coupling in hybrid lead halide perovskites, *Nature Communications* **7**, 11755 (2016).
- [13] M. Rini, R. Tobey, N. Dean, J. Itatani, Y. Tomioka, Y. Tokura, R. W. Schoenlein, and A. Cavalleri, Control of the electronic phase of a manganite by mode-selective vibrational excitation, *Nature* **449**, 72 (2007).
- [14] M. Mitrano, A. Cantaluppi, D. Nicoletti, S. Kaiser, A. Perucchi, S. Lupi, P. Di Pietro, D. Pontiroli, M. Riccò, S. R. Clark, D. Jaksch, and A. Cavalleri, Possible light-induced superconductivity in K_3C_{60} at high temperature, *Nature* **530**, 461 (2016).
- [15] M. Malinauskas, A. Žukauskas, S. Hasegawa, Y. Hayasaki, V. Mizeikis, R. Buividas, and S. Juodkazis, Ultrafast laser processing of materials: from science to industry, *Light: Science & Applications* **5**, e16133 (2016).
- [16] R. Mankowsky, M. Först, and A. Cavalleri, Non-equilibrium control of complex solids by nonlinear phonons, *Reports on Progress in Physics* **79**, 064503 (2016).
- [17] R. J. McQueeney, J. L. Sarrao, P. G. Pagliuso, P. W. Stephens, and R. Osborn, Mixed lattice and electronic states in high-temperature superconductors, *Phys. Rev. Lett.* **87**, 077001 (2001).
- [18] S. Tajima, Y. Fudamoto, T. Kakeshita, B. Gorshunov, V. Železný, K. M. Kojima, M. Dressel, and S. Uchida, In-plane optical conductivity of $La_{2-x}Sr_xCuO_4$: Reduced superconducting condensate and residual Drude-like response, *Phys. Rev. B* **71**, 094508 (2005).
- [19] L. Perfetti, P. A. Loukakos, M. Lisowski, U. Bovensiepen, H. Berger, S. Biermann, P. S. Cornaglia, A. Georges, and M. Wolf, Time evolution of the electronic structure of 1T-TaS₂ through the insulator-metal transition, *Phys. Rev. Lett.* **97**, 067402 (2006).
- [20] S. Hellmann, M. Beye, C. Sohrt, T. Rohwer, F. Sorgenfrei, H. Redlin, M. Källäne, M. Marczyński-Bühlow, F. Hennies, M. Bauer, A. Föhlisch, L. Kipp, W. Wurth, and K. Rossnagel, Ultrafast melting of a charge-density wave in the mott insulator 1T-TaS₂, *Phys. Rev. Lett.* **105**, 187401 (2010).
- [21] S. Hellmann, T. Rohwer, M. Källäne, K. Hanff, C. Sohrt, A. Stange, A. Carr, M. M. Murnane, H. C. Kapteyn, L. Kipp, M. Bauer, and K. Rossnagel, Time-domain classification of charge-density-wave insulators, *Nature Communications* **3**, 1069 (2012).
- [22] T. Rohwer, S. Hellmann, M. Wiesenmayer, C. Sohrt, A. Stange, B. Slomski, A. Carr, Y. Liu, L. M. Avila, M. Källäne, S. Mathias, L. Kipp, K. Rossnagel, and M. Bauer, Collapse of long-range charge order tracked by time-resolved photoemission at high momenta, *Nature* **471**, 490 (2011).
- [23] C.-K. Chan, T. E. Lee, and S. Gopalakrishnan, Limit-cycle phase in driven-dissipative spin systems, *Phys. Rev.*

- A **91**, 051601 (2015).
- [24] R. M. Wilson, K. W. Mahmud, A. Hu, A. V. Gorshkov, M. Hafezi, and M. Foss-Feig, Collective phases of strongly interacting cavity photons, *Phys. Rev. A* **94**, 033801 (2016).
- [25] M. Yarmohammadi, C. Meyer, B. Fauseweh, B. Normand, and G. S. Uhrig, Dynamical properties of a driven dissipative dimerized $S = \frac{1}{2}$ chain, *Phys. Rev. B* **103**, 045132 (2021).
- [26] M. Schiró, C. Joshi, M. Bordyuh, R. Fazio, J. Keeling, and H. E. Türeci, Exotic attractors of the nonequilibrium Rabi-Hubbard model, *Phys. Rev. Lett.* **116**, 143603 (2016).
- [27] J. Jin, D. Rossini, R. Fazio, M. Leib, and M. J. Hartmann, Photon solid phases in driven arrays of nonlinearly coupled cavities, *Phys. Rev. Lett.* **110**, 163605 (2013).
- [28] J. Jin, D. Rossini, M. Leib, M. J. Hartmann, and R. Fazio, Steady-state phase diagram of a driven qd-cavity array with cross-Kerr nonlinearities, *Phys. Rev. A* **90**, 023827 (2014).
- [29] T. E. Lee, H. Häffner, and M. C. Cross, Antiferromagnetic phase transition in a nonequilibrium lattice of Rydberg atoms, *Phys. Rev. A* **84**, 031402 (2011).
- [30] M. Marcuzzi, E. Levi, S. Diehl, J. P. Garrahan, and I. Lesanovsky, Universal nonequilibrium properties of dissipative Rydberg gases, *Phys. Rev. Lett.* **113**, 210401 (2014).
- [31] C. D. Parmee and N. R. Cooper, Phases of driven two-level systems with nonlocal dissipation, *Phys. Rev. A* **97**, 053616 (2018).
- [32] R. Labouvie, B. Santra, S. Heun, and H. Ott, Bistability in a driven-dissipative superfluid, *Phys. Rev. Lett.* **116**, 235302 (2016).
- [33] M. Foss-Feig, P. Niroula, J. T. Young, M. Hafezi, A. V. Gorshkov, R. M. Wilson, and M. F. Maghrebi, Emergent equilibrium in many-body optical bistability, *Phys. Rev. A* **95**, 043826 (2017).
- [34] M. Biondi, G. Blatter, H. E. Türeci, and S. Schmidt, Nonequilibrium gas-liquid transition in the driven-dissipative photonic lattice, *Phys. Rev. A* **96**, 043809 (2017).
- [35] J. Bonča and S. A. Trugman, Dynamic properties of a polaron coupled to dispersive optical phonons, *Phys. Rev. B* **103**, 054304 (2021).
- [36] D. M. Kennes, E. Y. Wilner, D. R. Reichman, and A. J. Millis, Transient superconductivity from electronic squeezing of optically pumped phonons, *Nature Physics* **13**, 479 (2017).
- [37] J. Sous, B. Kloss, D. M. Kennes, D. R. Reichman, and A. J. Millis, Phonon-induced disorder in dynamics of optically pumped metals from nonlinear electron-phonon coupling, *Nature Communications* **12**, 5803 (2021).
- [38] See the Supplemental Materials at <http://xxx.yyy.zzz> for further details of the model Hamiltonian, corresponding equations of motion, resonance/off-resonance phononic and electronic responses, and energy flows.
- [39] T. K. Kim, A. A. Kordyuk, S. V. Borisenko, A. Koitzsch, M. Knupfer, H. Berger, and J. Fink, Doping dependence of the mass enhancement in $(\text{Pb,Bi})_2\text{Sr}_2\text{CaCu}_2\text{O}_8$ at the antinodal point in the superconducting and normal states, *Phys. Rev. Lett.* **91**, 167002 (2003).
- [40] M. A. Sentef, Light-enhanced electron-phonon coupling from nonlinear electron-phonon coupling, *Phys. Rev. B* **95**, 205111 (2017).
- [41] M. Puviani and M. A. Sentef, Quantum nonlinear phononics route towards nonequilibrium materials engineering: Melting dynamics of a ferroelectric charge density wave, *Phys. Rev. B* **98**, 165138 (2018).
- [42] G. Lindblad, On the generators of quantum dynamical semigroups, *Comm. Math. Phys.* **48**, 119 (1976).
- [43] H. Breuer and F. Petruccione, *The Theory of Open Quantum Systems* (OUP Oxford, 2007).
- [44] M. Mitrano, G. Cotugno, S. R. Clark, R. Singla, S. Kaiser, J. Stähler, R. Beyer, M. Dressel, L. Baldassarre, D. Nicoletti, A. Perucchi, T. Hasegawa, H. Okamoto, D. Jaksch, and A. Cavalleri, Pressure-dependent relaxation in the photoexcited mott insulator $\text{ET-F}_2\text{TCNQ}$: Influence of hopping and correlations on quasiparticle recombination rates, *Phys. Rev. Lett.* **112**, 117801 (2014).
- [45] Z. Duan-Ming, F. Ran-Ran, L. Zhi-Hua, G. Li, L. Li, T. Xin-Yu, L. Dan, L. Gao-Bin, and H. De-Zhi, A new synthetic model of high-power pulsed laser ablation, *Communications in Theoretical Physics* **48**, 163 (2007).
- [46] E. Rowe, B. Yuan, M. Buzzi, G. Jotzu, Y. Zhu, M. Fechner, M. Först, B. Liu, D. Pontiroli, M. Riccò, and A. Cavalleri, Giant resonant enhancement for photo-induced superconductivity in K_3C_{60} (2023).
- [47] E. Wang, J. D. Adelinia, M. Chavez-Cervantes, T. Matsuyama, M. Fechner, M. Buzzi, G. Meier, and A. Cavalleri, Nonlinear transport in a photo-induced superconductor (2023).
- [48] P. E. Dolgirev, A. Zong, M. H. Michael, J. B. Curtis, D. Podolsky, A. Cavalleri, and E. Demler, Periodic dynamics in superconductors induced by an impulsive optical quench, *Communications Physics* **5**, 234 (2022).
- [49] A. von Hoegen, M. Fechner, M. Först, N. Taherian, E. Rowe, A. Ribak, J. Porras, B. Keimer, M. Michael, E. Demler, and A. Cavalleri, Amplification of superconducting fluctuations in driven $\text{YBa}_2\text{Cu}_3\text{O}_{6+x}$, *Phys. Rev. X* **12**, 031008 (2022).
- [50] M. Henstridge, M. Först, E. Rowe, M. Fechner, and A. Cavalleri, Nonlocal nonlinear phononics, *Nature Physics* **18**, 457 (2022).
- [51] M. Buzzi, D. Nicoletti, S. Fava, G. Jotzu, K. Miyagawa, K. Kanoda, A. Henderson, T. Siegrist, J. A. Schlueter, M.-S. Nam, A. Ardavan, and A. Cavalleri, Phase diagram for light-induced superconductivity in $\kappa\text{-(ET)}_2\text{-X}$, *Phys. Rev. Lett.* **127**, 197002 (2021).
- [52] M. Buzzi, G. Jotzu, A. Cavalleri, J. I. Cirac, E. A. Demler, B. I. Halperin, M. D. Lukin, T. Shi, Y. Wang, and D. Podolsky, Higgs-mediated optical amplification in a nonequilibrium superconductor, *Phys. Rev. X* **11**, 011055 (2021).
- [53] M. Buzzi, D. Nicoletti, M. Fechner, N. Tancogne-Dejean, M. A. Sentef, A. Georges, T. Biesner, E. Uykur, M. Dressel, A. Henderson, T. Siegrist, J. A. Schlueter, K. Miyagawa, K. Kanoda, M.-S. Nam, A. Ardavan, J. Coulthard, J. Tindall, F. Schlawin, D. Jaksch, and A. Cavalleri, Photomolecular high-temperature superconductivity, *Phys. Rev. X* **10**, 031028 (2020).
- [54] Note that the phonon relaxation is not modified because it remains gapped throughout the simulations at zero temperature.
- [55] R. Dann, A. Levy, and R. Kosloff, Time-dependent Markovian quantum master equation, *Phys. Rev. A* **98**, 052129 (2018).
- [56] S. L. Johnson, P. Beaud, E. Vorobeva, C. J. Milne,

- E. D. Murray, S. Fahy, and G. Ingold, Directly observing squeezed phonon states with femtosecond x-ray diffraction, *Phys. Rev. Lett.* **102**, 175503 (2009).
- [57] F. A. Lindemann, The calculation of molecular vibration frequencies, *Phys. Z.* **11**, 609 (1910).
- [58] D. Seipt, V. Y. Kharin, and S. G. Rykovanov, Optimizing laser pulses for narrow-band inverse Compton sources in the high-intensity regime, *Phys. Rev. Lett.* **122**, 204802 (2019).
- [59] V. Y. Kharin, D. Seipt, and S. G. Rykovanov, Higher-dimensional caustics in nonlinear Compton scattering, *Phys. Rev. Lett.* **120**, 044802 (2018).
- [60] C. J. Eckhardt, S. Chattopadhyay, D. M. Kennes, E. A. Demler, M. A. Sentef, and M. H. Michael, Theory of resonantly enhanced photo-induced superconductivity (2023).
- [61] S. Chattopadhyay, C. J. Eckhardt, D. M. Kennes, M. A. Sentef, D. Shin, A. Rubio, A. Cavalleri, E. A. Demler, and M. H. Michael, Mechanisms for long-lived, photo-induced superconductivity (2023).
- [62] F. Schlawin, D. M. Kennes, and M. A. Sentef, Cavity quantum materials, *Applied Physics Reviews* **9**, 011312 (2022).
- [63] M. A. Sentef, M. Ruggenthaler, and A. Rubio, Cavity quantum-electrodynamical polaritonically enhanced electron-phonon coupling and its influence on superconductivity, *Science Advances* **4**, eaau6969 (2018).
- [64] B. L. Dé, C. J. Eckhardt, D. M. Kennes, and M. A. Sentef, Cavity engineering of Hubbard U via phonon polaritons, *Journal of Physics: Materials* **5**, 024006 (2022).

Supplemental Materials for “Nonequilibrium phononic phase transition in a driven fermion chain”

Mohsen Yarmohammadi, Marin Bukov, and Michael H. Kolodrubetz

S1. HAMILTONIAN MODEL IN k -SPACE

In this section, we transfer the model in Eq. (1) into the reciprocal space. We apply the following Fourier transformations for both electronic (characterized by mode k) and phononic (characterized by mode q) sectors, $c_\ell^\dagger = L^{1/2} \sum_k \exp(-ik\ell) c_k^\dagger$ and $a_\ell^\dagger = L^{1/2} \sum_q \exp(-iq\ell) a_q^\dagger$. With this, the electronic dispersion is given by $\omega_k = -2t_0 \cos(k)$. As the first approximation, we consider the infrared active phonons as well as we only take into account the dispersionless $q = 0$ phonon mode. The physical reason behind the zero-momentum phonon mode approximation can be understood from the fact that the atoms generating the phonons in a lattice are of the order of Angstroms, while the laser wavelengths are of the order of nanometers. From this separation of scales, the zero phonon mode dominates. It can also be justified by the fact that in most materials the average phonon frequency is much larger than the phonon bandwidth. Thus, the total Hamiltonian reads

$$\mathcal{H} = \sum_k \omega_k c_k^\dagger c_k + \omega_0 a_0^\dagger a_0 + \frac{g_q}{L} (a_0^\dagger + a_0)^2 \sum_k (c_k^\dagger c_k - \langle c_k^\dagger c_k \rangle_{\text{eq}}) + \mathcal{E}(t) \sqrt{L} (a_0^\dagger + a_0), \quad (\text{S1})$$

where k belongs to the Brillouin zone from $-\pi$ to π for a lattice constant $l_0 = 1$. Moreover, $L^{-1} \sum_k \langle c_k^\dagger c_k \rangle_{\text{eq}} = 1/2$ is the equilibrium value of electron density.

S2. PHYSICAL OBSERVABLES AND QUANTUM MASTER EQUATIONS

In this section, we define the physical observables and the corresponding expectation values for both electronic and phononic sectors as

$$q_{\text{ph}}(t) = \langle \frac{1}{\sqrt{L}} (a_0^\dagger + a_0) \rangle(t) := \text{phonon displacement}, \quad (\text{S2a})$$

$$p_{\text{ph}}(t) = \langle \frac{i}{\sqrt{L}} (a_0^\dagger - a_0) \rangle(t) := \text{phonon momentum}, \quad (\text{S2b})$$

$$n_{\text{ph}}(t) = \langle \frac{1}{L} a_0^\dagger a_0 \rangle(t) := \text{phonon occupation}, \quad (\text{S2c})$$

$$Q_{\text{ph}}(t) = \langle \frac{1}{L} (a_0^\dagger a_0^\dagger + a_0 a_0) \rangle(t) := \text{squeezed-phonon displacement}, \quad (\text{S2d})$$

$$P_{\text{ph}}(t) = \langle \frac{i}{L} (a_0^\dagger a_0^\dagger - a_0 a_0) \rangle(t) := \text{squeezed-phonon momentum}, \quad (\text{S2e})$$

$$n_{e,k}(t) = \langle c_k^\dagger c_k \rangle(t) := k\text{-component of electron number}. \quad (\text{S2f})$$

Before turning to the ordinary differential equations of motion (EoM), it is also useful to define the electron density

$$n_e(t) = \frac{1}{L} \sum_k n_{e,k}(t) \quad (\text{S3})$$

for which the constraint $n_e(t) \leq 1/2$ should be hold in the presence of quadratic electron-phonon coupling (QEPC) g_q . We would also mention that Lindemann’s criterion [57] provides an estimate for the phonon occupation $n_{\text{ph}}(t) \lesssim 1$ to avoid lattice melting in a solid state system. This is also satisfied in our simulations.

Now we take the role of dampings into account. To do so, we use the adjoint quantum master equation for an arbitrary observable $O(t)$ in an open system for which the Heisenberg equation of motion is extended to deduce the time evolution of the entire system [42, 43]. The equation describing the coherent evolution and the dissipator reads

$$\langle \dot{O} \rangle(t) = i \langle [\mathcal{H}, O(t)] \rangle + \frac{1}{2} \sum_\ell \gamma_\ell \langle [\mathcal{L}_\ell^\dagger, O(t)] \mathcal{L}_\ell + \mathcal{L}_\ell^\dagger [O(t), \mathcal{L}_\ell] \rangle, \quad (\text{S4})$$

where the summation ℓ runs over all possible states in the Hilbert space and \mathcal{L}_ℓ are the time-independent Lindblad jump operators in the reduced system's Liouville space. The damping parameters are γ_{ph} and γ_e , respectively, for the phonon and electron.

The Heisenberg term, i.e. the first term of the above equation, is straightforward to be obtained for defined observables in Eq. (S2). Turning to the second term of Eq. (S4), the possible jump operators for the phononic sector can be each of $\mathcal{L}_\ell = a_0, a_0^\dagger, a_0 a_0^\dagger, a_0^\dagger a_0, a_0 a_0$, and $a_0^\dagger a_0^\dagger$. Let us label the corresponding damping parameters with $\gamma_1, \gamma_2, \gamma_3, \gamma_4, \gamma_5$, and γ_6 , respectively. Since the environment is supposed to be the same for all these channels, one can rewrite the above damping parameters as $\gamma_{\text{ph}} r_1, \gamma_{\text{ph}} r_2, \gamma_{\text{ph}} r_3, \gamma_{\text{ph}} r_4, \gamma_{\text{ph}} r_5$, and $\gamma_{\text{ph}} r_6$, respectively, in which $r_{\{1, \dots, 6\}}$ refer to the arrival rates of states after interacting with the phononic bath. For the two first operators, since the weak interaction with many atoms is supposed to simulate the coupling to a thermal bath (Markovian approximation) with temperature T , the rates r_1 and r_2 must be related to each other by a Maxwell-Boltzmann factor, i.e.

$$\frac{r_2}{r_1} = e^{-\tilde{\omega}_0(t)/k_{\text{B}}T} = \frac{\mathcal{N}_0(t)}{1 + \mathcal{N}_0(t)}, \quad (\text{S5})$$

where $\mathcal{N}_0(t)$ is the mean number of energy quanta at time t in the phonon mode corresponding to the modulated frequency $\tilde{\omega}_0(t) = \omega_0 \sqrt{1 + 4g_{\text{q}} \Delta n_{\text{e}}(t) / \omega_0}$, where $\Delta n_{\text{e}}(t) = n_{\text{e}}(t) - 1/2$ [55]. As for the cases $a_0^\dagger a_0$ and $a_0 a_0^\dagger$, the corresponding states have the same arrival rates because they are not acting as ladder operators and do not change the states when interacting, thus, $r_4/r_3 = 1$. For the two last cases, however, we neglect order operators higher than bilinear and set their contribution to zero in the dissipation process, i.e. $r_5 = r_6 = 0$. Considering Eq. (S4), after pretty straightforward calculations, the only Lindblad operators contributing to the dissipation effects originate from the non-conserving phonon operators, a_0 and a_0^\dagger , described by Eq. (S5).

Finally, in order to make these coupled equations solvable, we use a mean-field approximation in which entanglement between electronic and phononic degrees of freedom are neglected. With these approximations, we then obtain the time evolution of the phononic observables as

$$\dot{q}_{\text{ph}}(t) = +\omega_0 p_{\text{ph}}(t) - \frac{\gamma_{\text{ph}}}{2} [1 + 2\mathcal{N}_0(t)] q_{\text{ph}}(t), \quad (\text{S6a})$$

$$\dot{p}_{\text{ph}}(t) = -[\omega_0 + 4g_{\text{q}} \Delta n_{\text{e}}(t)] q_{\text{ph}}(t) - 2\mathcal{E}(t) - \frac{\gamma_{\text{ph}}}{2} [1 + 2\mathcal{N}_0(t)] p_{\text{ph}}(t), \quad (\text{S6b})$$

$$\dot{n}_{\text{ph}}(t) = -\mathcal{E}(t) p_{\text{ph}}(t) - 2g_{\text{q}} \Delta n_{\text{e}}(t) \mathcal{P}_{\text{ph}}(t) - \gamma_{\text{ph}} [n_{\text{ph}}(t) - \mathcal{N}_0(t)], \quad (\text{S6c})$$

$$\dot{\mathcal{Q}}_{\text{ph}}(t) = +2[\omega_0 + 2g_{\text{q}} \Delta n_{\text{e}}(t)] \mathcal{P}_{\text{ph}}(t) + 2\mathcal{E}(t) p_{\text{ph}}(t) - \gamma_{\text{ph}} [\mathcal{Q}_{\text{ph}}(t) - \mathcal{N}_0(t)], \quad (\text{S6d})$$

$$\dot{\mathcal{P}}_{\text{ph}}(t) = -2[\omega_0 + 2g_{\text{q}} \Delta n_{\text{e}}(t)] \mathcal{Q}_{\text{ph}}(t) - 2\mathcal{E}(t) q_{\text{ph}}(t) - 4g_{\text{q}} [2n_{\text{ph}}(t) + 1/L] \Delta n_{\text{e}}(t) - \gamma_{\text{ph}} [\mathcal{P}_{\text{ph}}(t) - \mathcal{N}_0(t)]. \quad (\text{S6e})$$

As the laser drive is what takes us out of equilibrium, there is no displacement/movement for the phononic sector in equilibrium, leading to the initial conditions $O_{\text{ph}}(0) = 0$.

For the single electron $O(t) = n_{e,k}(t)$, we again consider all possible Lindblad operators $c_k, c_k^\dagger, c_k c_k^\dagger$, and $c_k^\dagger c_k$. Again, we do not consider higher order terms including electron-electron interaction and would obtain bilinear EoMs. Then, the arrival rates of states to the electron after interacting with the phononic bath follow the same argument as

$$\frac{r_2}{r_1} = e^{-\tilde{\omega}_k(t)/k_{\text{B}}T} = \frac{\mathcal{N}_k(t)}{1 - \mathcal{N}_k(t)}, \quad (\text{S7})$$

where $\mathcal{N}_k(t)$ is the mean number of energy quanta at time t in the electron mode corresponding to the modulated dispersion $\tilde{\omega}_k(t) = \omega_k + g_{\text{q}} q_{\text{ph}}^2(t)$ [55]. The fact that QEPC acts as a chemical potential in the electronic dispersion stems from the fact that the phonon is coupled to the local electron number in our model, leading to a shift in the electron energy.

Within the same manner, the electron conserving jump operators $c_k c_k^\dagger, c_k^\dagger c_k$ lead to zero contributions to the dynamical properties of electron ($r_4/r_3 = 1$). Ultimately, the time evolution of the electron number is obtained as

$$\dot{n}_{e,k}(t) = -\gamma_e [n_{e,k}(t) - \mathcal{N}_k(t)]. \quad (\text{S8})$$

As an extension to the model, placing material into an optical cavity can be considered to circumvent detrimental heating, which is a fundamental problem for driving materials with classical light. This, in turn, enhances the light-matter coupling for which a few photon states of the cavity can influence the matter's degrees of freedom [62]. Generally, to treat both light and matter quantum mechanically, one has to deal with host hybrid states as a mixture of both light and matter degrees of freedom. For instance, it has been proposed that coupling cavity modes to the phonons involved in electronic pairing [63] or by directly coupling to the electronic degrees of freedom, the superconductivity in a cavity can be influenced [64].

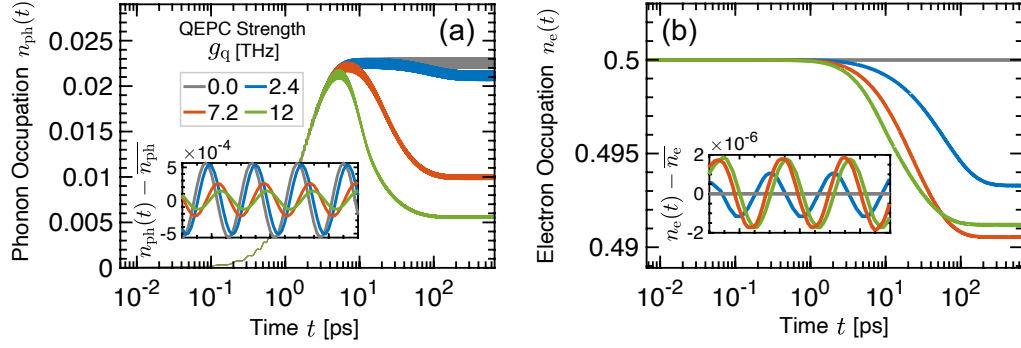


FIG. S3. Time evolution of dressed (a) phonon and (b) electron occupations for various QEPCs at $\mathcal{A}_0 = 0.038$, resonant $\omega = \omega_0 = 4.8$, $\gamma_{\text{ph}} = 0.24$, and $\gamma_e = 0.0024$ (all units are THz). Both sectors show a frequency doubling effect (inset panels) in the NESS accompanied by a phase shift φ due to QEPC.

S3. NONEQUILIBRIUM STEADY STATE

To establish the nonequilibrium steady state (NESS) by steady laser driving, we first investigate the evolution of the resonance ($\omega = \omega_0$) phononic and electronic responses upon tuning the QEPC across the nonequilibrium, as shown in Fig. S3. Due to the weak coupling of a single Einstein phonon to an ensemble of phonons (bath), we set phonon damping rate γ_{ph} to a value of order 5% of the phonon energy, consistent with the experimental recombination rates of certain quasi-1D Mott insulators [44]. Further, the electron mode is in general damped to a phononic bath weaker than Einstein phonon, i.e., $\gamma_e < \gamma_{\text{ph}}$, and accordingly we set γ_e to a value of order 0.1% of the electron hopping energy.

Phonon occupation pumps into a steady state exponentially due to the laser field and reaches the NESS at approximately four-time constants of the phonon system $2/\gamma_{\text{ph}}$. From the fact that the power of the laser is proportional to the squared amplitude of the laser field, the plateau value of decoupled phase $g_q = 0$ reaches $(\mathcal{A}_0/\gamma_{\text{ph}})^2$ similar to a damped driven harmonic oscillator, in agreement with Ref. [25]. For $g_q = 0$, the electron number displays the equilibrium plateau $1/2$. For $g_q \neq 0$, a NESS forms with deviations in phononic and electronic plateaus stemming from the feedback between nonequilibrium phonons and dressed electronic dispersion $\tilde{\omega}_k(t) = \omega_k + g_q q_{\text{ph}}^2(t)$. Subtracting averages from the time evolutions in the NESS gives rise to trackable oscillations, as shown in inset panels of Figs. S3(a) and S3(b). The point refers to the oscillation frequency; both quantities oscillate with the frequency $2\omega_0$ – frequency doubling effect – in the NESS accompanied by a phase shift φ due to QEPC. As an explanation, the decrease (increase) in the amplitude of NESS for the phonon (electron) sector with QEPC is a standard consequence of energy level repulsion.

S4. ENERGY FLOWS THROUGH THE ELECTRON-PHONON SYSTEM

In this section, we intend to focus on the energies per unit of time in the model. For a better understanding of the presented energy flows in the following, we draw Fig. S4(a) to track the context. The input energy $\mathcal{J}^{1 \rightarrow \text{p}}$ is due to the laser field, which goes into the driven phonon. The driven phonon splits this input energy into the energy entering the QEPC part and the phononic bath, given respectively by $\mathcal{J}^{\text{p} \rightarrow \text{QEPC}}$ and $\mathcal{J}^{\text{p} \rightarrow \text{b}}$. The energy entering the QEPC part is again divided into two parts $\mathcal{J}^{\text{QEPC} \rightarrow \text{e}}$ and $\mathcal{J}^{\text{QEPC} \rightarrow \text{b}}$ referring, respectively, to the energy entering the electron and the bath. Finally, the electron induces the energy flow of $\mathcal{J}^{e \rightarrow \text{b}}$ to the bath through the dissipation. These powers can directly be obtained from the EoMs of phonon occupation and electron number in Eqs. (S6c) and (S8):

$$\mathcal{J}^{1 \rightarrow \text{p}}(t) = -\mathcal{E}(t)\omega_0 p_{\text{ph}}(t), \quad (\text{S9a})$$

$$\mathcal{J}^{\text{p} \rightarrow \text{QEPC}}(t) = +2g_q \omega_0 \Delta n_e(t) \mathcal{P}_{\text{ph}}(t), \quad (\text{S9b})$$

$$\mathcal{J}^{\text{p} \rightarrow \text{b}}(t) = +\gamma_{\text{ph}} \omega_0 n_{\text{ph}}(t), \quad (\text{S9c})$$

$$\mathcal{J}^{\text{QEPC} \rightarrow \text{b}}(t) = +g_q [\gamma_e + \gamma_{\text{ph}}] \Delta n_e(t) q_{\text{ph}}^2(t), \quad (\text{S9d})$$

$$\mathcal{J}^{\text{QEPC} \rightarrow \text{e}}(t) = +g_q q_{\text{ph}}^2(t) \gamma_e \left[\frac{1}{2} - \frac{1}{L} \sum_k \mathcal{N}_k(t) \right], \quad (\text{S9e})$$

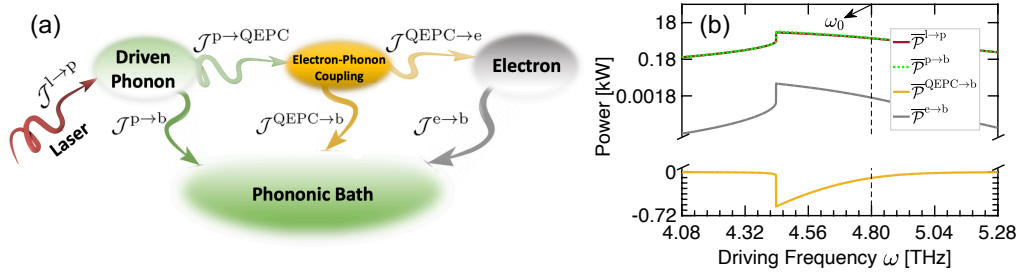


FIG. S4. (a) Schematic picture of the energy flows within a driven-dissipative fermionic chain; $\mathcal{J}^{l \rightarrow p}$ is the uptake of laser energy by the driven phonon, $\mathcal{J}^{p \rightarrow \text{QEPC}}$ is energy flowing out of the driven phonon due to the presence of the QEPC, and $\mathcal{J}^{p \rightarrow b}$ is the energy flowing from the driven phonon and directly to the phononic bath. Furthermore, $\mathcal{J}^{\text{QEPC} \rightarrow e}$ and $\mathcal{J}^{\text{QEPC} \rightarrow b}$ are, respectively, the energy flowing out of the QEPC part to the electron and bath. Finally, the electron induces the energy flow of $\mathcal{J}^{e \rightarrow b}$ to the bath through the dissipation. (b) Input and output powers through the electron-phonon system with the same parameters as Fig. 2(a) and Fig. 2(b) for $g_q/\omega_0 = 2$. Total power sum rule $\overline{\mathcal{J}}^{l \rightarrow p} = \overline{\mathcal{J}}^{p \rightarrow b} + \overline{\mathcal{J}}^{\text{QEPC} \rightarrow b} + \overline{\mathcal{J}}^{e \rightarrow b}$ is evident from the driving to the final stage of dissipation.

$$\mathcal{J}^{e \rightarrow b}(t) = + \frac{\gamma_e}{L} \sum_k \omega_k [n_{e,k}(t) - \mathcal{N}_k(t)]. \quad (\text{S9f})$$

Although most of the above expressions are clear from the EoMs, Eq. (S9d) needs more clarification: $\mathcal{J}^{\text{QEPC} \rightarrow b}(t)$ is obtained using the time-derivative of QEPC Hamiltonian in Eq. (S1) via

$$\frac{1}{L} \partial_t \langle \mathcal{H}_{e-\text{ph}} \rangle(t) = \partial_t [g_q q_{\text{ph}}^2(t) \Delta n_e(t)] = \mathcal{J}^{p \rightarrow \text{QEPC}}(t) - [\mathcal{J}^{\text{QEPC} \rightarrow b}(t) + \mathcal{J}^{\text{QEPC} \rightarrow e}(t)], \quad (\text{S10})$$

which the very small energy entering the electron from the QEPC part is stemming from the reflection of the dressed electronic dispersion from the bath to the QEPC subsystem.

Having the explicit form of energy flows, we can explore the physical sum rules which should be valid at each stage. It should be noted that, after taking the average of the late-time signals over one period, the input energy from the laser driving field should satisfy $\overline{\mathcal{J}}^{l \rightarrow p} = \overline{\mathcal{J}}^{p \rightarrow b} + \overline{\mathcal{J}}^{\text{QEPC} \rightarrow b} + \overline{\mathcal{J}}^{e \rightarrow b}$ in the NESS, originating from the energy conservation. In addition to this general sum rule, three further rules are valid for the subprocesses: (i) $\overline{\mathcal{J}}^{l \rightarrow p} = \overline{\mathcal{J}}^{p \rightarrow \text{QEPC}} + \overline{\mathcal{J}}^{p \rightarrow b}$, (ii) $\overline{\mathcal{J}}^{p \rightarrow \text{QEPC}} = \overline{\mathcal{J}}^{\text{QEPC} \rightarrow e} + \overline{\mathcal{J}}^{\text{QEPC} \rightarrow b}$ and (iii) $\overline{\mathcal{J}}^{\text{QEPC} \rightarrow e} = \overline{\mathcal{J}}^{e \rightarrow b}$.

Finally, with the help of energy flows, one can use a sample with a thickness w , area a , and the molar density ρ to obtain the power in kW as

$$\mathcal{P}^{\text{O} \rightarrow \square}(t) = w a \rho \mathcal{J}^{\text{O} \rightarrow \square}(t). \quad (\text{S11})$$

The input energy fluence $\mathcal{P}^{l \rightarrow p}$ due to the laser field excites the phonon and it is an absorbance spectrum proportional to the phonon occupation, as shown in Fig. S4(b). The net energy flow bears a close resemblance to Figs. S3(a) and S3(b) with additional weighting factors of ω_0 and ω_k (see Eq. S9 of the SM). It can be seen that the majority of the laser energy flows directly to the phononic bath and a relatively tiny fraction of it (negligible) can be absorbed by the electron. Moreover, the negative sign of $\overline{\mathcal{P}}^{\text{QEPC} \rightarrow b}$ implies a small energy flow from the bath due to the QEPC term. Therefore such an absorbance can be used for quantitative analysis. In Fig. S4(b), one may compute the net power in the NESS, $\overline{\mathcal{P}}^{p \rightarrow b} + \overline{\mathcal{P}}^{\text{QEPC} \rightarrow b} + \overline{\mathcal{P}}^{e \rightarrow b}$, which by the sum rules at each step matches $\overline{\mathcal{P}}^{l \rightarrow p}$ for energy conservation.

S5. EFFECTIVE FORCE TREATMENT OF THE NONEQUILIBRIUM PHASE TRANSITION

As the input laser drive is a continuous wave field, the output coherent oscillations in the NESS must synchronize with it. To understand the phase shift caused by QEPC, we Fourier decompose the phonon oscillations in the NESS, $q_{\text{ph}}^{\text{NESS}}(t) = \sum_n q_n e^{i n \omega t}$ and substitute it in Eqs. (S6a) and (S6b), leading to (at $T = 0$, $\mathcal{N}_0(t) \rightarrow 0$)

$$i n \omega q_n = \omega_0 p_n - \frac{\gamma_{\text{ph}}}{2} q_n, \quad (\text{S12a})$$

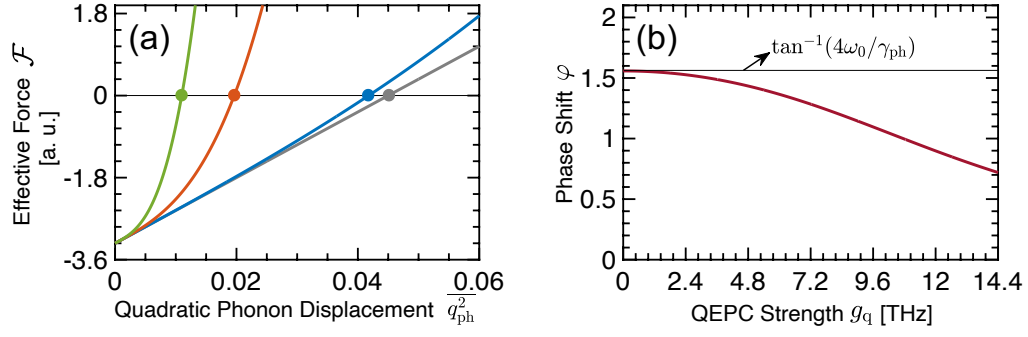


FIG. S5-1. (a) Effective force $\mathcal{F}(\mathcal{X})$, Eq (S14a), with $\mathcal{X} = \overline{q_{\text{ph}}^2}$ for various QEPCs. (b) Deviation from the decoupled phase shift, i.e. $\arctan(4\omega_0/\gamma_{\text{ph}})$ observed in inset Figs. S3(a) and S3(b) in the NESS, is due to QEPC at $\mathcal{X} \simeq 0.0197$ (see the orange line in (a)).

$$in\omega p_n = -\omega_0 q_n - 4q_q \sum_{n'} n_{e,n'} q_{n-n'} + 2g_q q_n - 2\mathcal{A}_0 - \frac{\gamma_{\text{ph}}}{2} p_n, \quad (\text{S12b})$$

As seen in the numerics, the dominant harmonics are $n = 1$ for q_{ph} and $n' = 0$ for n_e (henceforth, we use the notation $n_{e,0} = \overline{n_e}$ since the zeroth Fourier harmonics is that of the averaged plateau in the NESS):

$$q_1 = \frac{2\mathcal{A}_0\omega_0}{\omega^2 - \omega_0^2 + \frac{\gamma_{\text{ph}}^2}{4} - 4g_q\omega_0(\overline{n_e} - 1/2) - i\gamma_{\text{ph}}\omega} = |q_1|e^{i\varphi}, \quad (\text{S13a})$$

$$|q_1| = \frac{2\mathcal{A}_0\omega_0}{\sqrt{[\omega^2 - \omega_0^2 + \frac{\gamma_{\text{ph}}^2}{4} - 4g_q\omega_0(\overline{n_e} - 1/2)]^2 + \gamma_{\text{ph}}^2\omega^2}}, \quad (\text{S13b})$$

$$\varphi = \arctan\left(\frac{\gamma_{\text{ph}}\omega}{\omega^2 - \omega_0^2 + \frac{\gamma_{\text{ph}}^2}{4} - 4g_q\omega_0(\overline{n_e} - 1/2)}\right). \quad (\text{S13c})$$

From a physical point of view, the driven phonon typically exhibits different characteristic behaviors far from equilibrium compared to equilibrium that are not generally described by a minimization principle. As we deal with a damped driven dressed (by the electron) harmonic oscillator, there is an effective force acting on the phonon and microscopically on $|q_1|$ far from equilibrium. This force can be obtained from setting $\ddot{q}_{\text{ph}} = \dot{q}_{\text{ph}} = 0$ in the NESS. Using the relations $\overline{q_{\text{ph}}^2} = |q_1|^2/2$ and $\overline{n_e} = 1/2 - g_q\overline{q_{\text{ph}}^2}/2\pi t_0$ stemming from the dressed Fermi momentum \tilde{k}_F , Eq. (S13b) can be rewritten as a cubic equation $\mathcal{F}(\mathcal{X}) = 0$ for $\mathcal{X} = \overline{q_{\text{ph}}^2}$, satisfying the physics behind the relative effective force (assuming atomic mass = 1) discussed above. Here we use this relative effective force to find $|q_1| = \sqrt{2\overline{q_{\text{ph}}^2}}$ required for the phase shift. Thus,

$$\mathcal{F}(\mathcal{X}) = a\mathcal{X}^3 + b\mathcal{X}^2 + c\mathcal{X} + d, \quad (\text{S14a})$$

$$a = -4\frac{g_q^4\omega_0^2}{\pi^2 t_0^2}, \quad b = -4\frac{g_q^2\omega_0}{\pi t_0}\left(\omega^2 - \omega_0^2 + \frac{\gamma_{\text{ph}}^2}{4}\right), \quad c = -\gamma_{\text{ph}}^2\omega^2 - (\omega^2 - \omega_0^2)^2, \quad d = 2\mathcal{A}_0^2\omega_0^2. \quad (\text{S14b})$$

As shown in Fig. S5-1(a), a single root appears for $\mathcal{F}(\mathcal{X})$ when the laser drive is in resonance with the phonon. This root should be plugged into $\overline{n_e}$ to find the phase shift φ at $\omega = \omega_0$, resulting in $\varphi(\mathcal{X}) = \arctan(\gamma_{\text{ph}}\omega_0/[\gamma_{\text{ph}}^2/4 + 2g_q^2\omega_0\mathcal{X}/\pi t_0])$, as shown in Fig. S5-1(b). This phase shift decreases with QEPC as the quadratic phonon displacement is decreased.

By analyzing $\mathcal{F}(\mathcal{X})$ diagram using Eq. (S14a) for off-resonance conditions, we can attribute the origin of phase transition to shifts of the cubic function, leading to creation/annihilation of roots. The off-resonance nonequilibrium dynamics of the spinless fermionic chain subject to a laser drive can broadly be divided into three regions depending on the QEPC strength, namely $\omega < \omega_c$, $\omega = \omega_c$, and $\omega > \omega_c$, where ω_c is the threshold driving frequency at which the phase transition takes place. For these regimes, we plot $\mathcal{F}(\mathcal{X})$ as a function of \mathcal{X} in Fig. S5-2(a). The extrema of $\mathcal{F}(\mathcal{X})$ from Eq. (S14a) occur when $d\mathcal{F}(\mathcal{X})/d\mathcal{X} = 0$, so, two stationary points locate at $\mathcal{X}_1 = -(b/3a) + \sqrt{\Delta}/6a$ and $\mathcal{X}_2 = -(b/3a) - \sqrt{\Delta}/6a$, where $\Delta = 4b^2 - 12ac$. From Eq. (S14b), a and c coefficients are always positive, while d is always negative. For $\omega < \omega_0$, b becomes negative, while it is positive at $\omega = \omega_0$ and $\omega > \omega_0$. Here we address $\omega < \omega_0$. For various driving frequencies in the current set of parameters, there is a critical $\omega = \omega_c = 4.44$ THz at which two

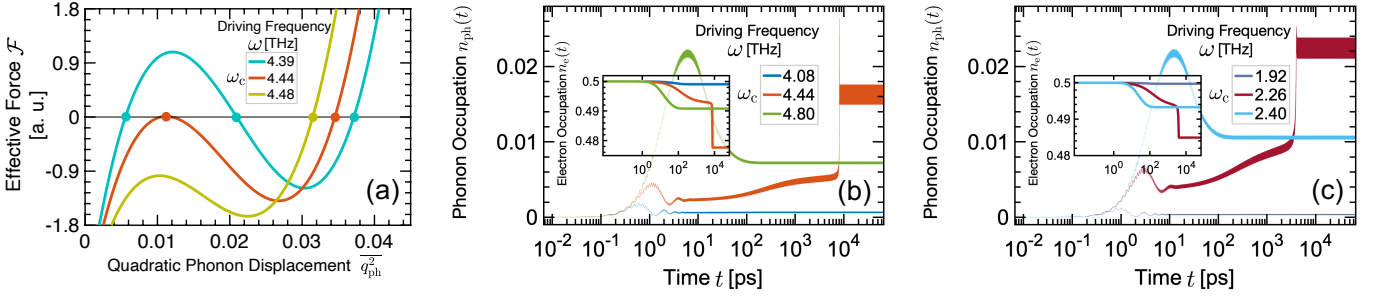


FIG. S5-2. (a) Effective force, Eq (S14a), characterized by $\mathcal{X} := \frac{\omega}{\omega_0}$ for off-resonance driving frequencies with the phonon frequency $\omega_0 = 4.8$ THz. The threshold driving frequency at which the phase transition occurs is $\omega_c = 4.44$ THz. Off-resonance time evolution of dressed phonon occupation (main panels) and electron number (inset panels) for phonon frequency (b) $\omega_0 = 4.8$ THz with $\omega_c = 4.44$ THz and (c) $\omega_0 = 2.4$ THz with $\omega_c = 2.26$ THz and three regimes of driving frequencies below, at, and above ω_c at $g_q/\omega_0 = 2$, $\mathcal{A}_0 = 0.038$, $\gamma_{\text{ph}} = 0.24$, and $\gamma_e = 0.0024$ (all units are THz).

of the three distinct roots become identical at $\text{Re}[\mathcal{X}_1]$. For $\omega < \omega_c$, the first and third roots are stable solutions, while the second root is unstable; it can be understood from the slopes around the roots. However, the first solution is the relevant physical one based on the nature of EoMs in our coupled model with a vacuum ground state. As an explanation, one would argue that the laser cannot strongly excite phonons at low frequencies (before the strongest response at the phase transition point) and the weakest phonon displacement is expected to be detected, which is that of the first solution. To physically interpret the behaviors at $\omega = \omega_c$, one would argue that the force acting on the phonon instantaneously vanishes and the pattern becomes static, hence, a sharp jump to the third root for restoring dynamic patterns happens. This is where the first-order phase transition emerges. For $\omega > \omega_c$, the third root is the only left one as we approach the phonon frequency $\omega_0 = 4.8$ THz.

To find the exact analytical expression for ω_c , we use the fact that, at $\omega = \omega_c$, the imaginary part of \mathcal{X}_1 for $\Delta < 0$ vanishes. Thus, one immediately finds $\omega_{\mathcal{X}_1} = \sqrt{\omega_0^2 + \frac{\gamma_{\text{ph}}^2}{2}} - \sqrt{3}\gamma_{\text{ph}}\omega_0$ to satisfy $\Delta < 0$. Afterwards, we obtain $\mathcal{X}_1 = -\tilde{b}|_{\omega_{\mathcal{X}_1}}/3a$ with

$$\tilde{b} = \frac{g_q^2 \omega_0 \gamma_{\text{ph}}}{\pi t_0} \left(3\gamma_{\text{ph}} - 4\sqrt{3}\omega_0 \right). \quad (\text{S15})$$

Due to the weak coupling of a single Einstein phonon to an ensemble of phonons (bath), $\gamma_{\text{ph}} < \omega_0$ always holds, implying that the above characteristic parameter \tilde{b} is physically always negative to have the expected positive $\mathcal{X}_1 = \frac{\omega}{\omega_0}$. Eventually, plugging $\mathcal{X}_1 = -\tilde{b}/3a$ into Eq. (S14a) yields the following solution for ω_c

$$\omega_c = \sqrt{\omega_0^2 - \frac{2\sqrt{3}}{3}\gamma_{\text{ph}}\omega_0 + \frac{1}{2}\sqrt{\gamma_{\text{ph}}^4 - \frac{\pi t_0 \tilde{b}}{3g_q^2 \omega_0} - 4\gamma_{\text{ph}}^2 \omega_0^2 - \frac{96g_q^4 \omega_0^4 \mathcal{A}_0^2}{\pi^2 t_0^2 \tilde{b}}}}. \quad (\text{S16})$$

For the set of parameters $\omega_0 = 4.8$, $g_q = 9.6$, $\mathcal{A}_0 = 0.038$, $\gamma_{\text{ph}} = 0.24$, and $\gamma_e = 0.0024$ (all units are THz), one exactly obtains $\omega_c = 4.44$ THz, in excellent agreement with above numerical findings.

It should be noted that the Lindblad approach applies in the Markovian limit of a weak system-bath coupling; this is contained not in the parameter g_q , but in the damping parameters γ_{ph} and γ_e . Technically, our treatment is entirely consistent with the requirements of the Lindblad formalism and no artifacts will arise. Therefore, having a large QEPC and a small damping rate in the same system is not a contradiction. Moreover, the breakdown of the lattice is still governed by the Lindemann criterion [57] through the connection between allowed phonon damping and weak laser amplitude in our model.

The corresponding time evolution of phonon occupation and electron number is also shown in Figs. S5-2(b) and S5-2(c) for two phonon frequencies. The phase shift analysis due to the presence of QEPC in the previous section is also valid here for $\omega \neq \omega_0$. For $\omega = \omega_c$ and sufficiently large QEPC ($g_q/\omega_0 = 2$), phonon occupation first rises to diverge but it pulls down again to another NESS plateau (largest value). At the same time, the electron number drops down to the lowest NESS plateau, as shown in the inset panels. The appearance of divergence spectrograms – first-order phase transition – at large QEPC is largely independent of the phonon frequency.